ORIGINAL RESEARCH PAPER

One-step Cathodic Electrochemical Synthesis and Characterization of Dextran Coated Magnetite Nanoparticles

Mustafa Aghazadeh [1]*, Isa Karimzadeh [2]

[1] *Materials and Nuclear Research School, Nuclear Science and Technology Research Institute (NSTRI), Tehran, Iran*

[2] *Department of Physics, Faculty of Science, Central Tehran Branch, Islamic Azad University, Tehran, Iran*

Received: 2017-08-07 Accepted: 2017-11-08 Published: 2017-12-01

ABSTRACT

In this research, a simple and efficient cathodic electrochemical deposition (CED) route was developed for the preparation of magnetite nanoparticles (NPs) in an aqueous media. The surface of magnetite NPs was also coated for the first time *via* an *in situ* procedure during the CED process. In this method, initially, the Fe_3O_4 NPs (with size ~10 nm) were prepared from the Fe^{2+}/Fe^{3+} chloride bath through CED process. Then, dextran as the coating agent was coated on the surface of Fe_3O_4 NPs during the CED process. The prepared NPs were characterized by different techniques such as XRD, FE-SEM, TEM, IR, TGA, DLS and VSM. The XRD results proved the pure magnetite i.e. Fe_3O_4 crystal phase of the prepared samples. Morphological observations through FE-SEM and TEM revealed particle morphology with nano-sizes of 8 nm and 12 nm for the naked and dextran coated NPs, respectively. The dextran coat on the surfaces of NPs was confirmed by FT-IR and DSC-TGA analyses. The average hydrodynamic diameters of 17 nm and 54 nm were measured from DLS analysis for the naked and dextran coated NPs, respectively. The magnetic analysis by VSM revealed that prepared NPs have superparamagnetic behavior, i.e. M_s=82.3 emu $g^{-1,}$ magnetization *Mr*=0.71 emug^{-1} and Ce=2.3 Oe for the naked NPs, and M_s=43.1 emu g^{-1}, *Mr*=0.47 emu g^{-1} and *Ce*=0.81Oe for the dextran coated NPs. These results implied that this electrochemical strategy can be recognized as an effective preparation method of polymer coated Fe_3O_4 NPs.

Keywords: *Magnetite; Nanoparticles; Cathodic Electrodeposition; In situ coating; Dextran*

How to cite this article

Aghazadeh M, Karimzadeh I. One-step Cathodic Electrochemical Synthesis and Characterization of Dextran Coated Magnetite Nanoparticles. J. Nanoanalysis., 2017; 4(3): 228-238. DOI: 10.22034/jna.2017.542007.1018

INTRODUCTION

During the last decade, superparamagnetic iron oxide nanoparticles (SPIONs) have potentially revolutionized the biomedical applications like as hyperthermia, drug delivery, magnetic resonance imaging (MRI) contrast agent, immunoassay, hyperthermia, cell separation and cancer therapy [1-4]. The small size of SPIONs leads to high surface area to volume ratio which provides an unprecedented size-dependent superparamagnetism property. Particles with the sizes of 10-20 nm generate the highest level of magnetization [5]. In SPIONs, surface energy can be reduced via agglomeration due to the high ratio of surface area to volume [6]. As agglomeration is a drawback of SPIONs' behavior, different coatings

* Corresponding Author Email: maghazadeh@aeoi.org.ir

such as stabilizing agents should be used to modify the surface of SPIONs. Therefore, the NPs which are used in all biomedical applications should have suitable surface coatings, high magnetization level, appropriate particle size (<100 nm), and a narrow distribution of particle size [7]. The surface coats of SPIONs with nontoxic and biocompatible materials affect their bio-distribution, cellular absorption, metabolism and blood circulation [8-11]. Also, surface coats have a great effect on the proficiency of SPIONs in biomedical uses. In this way, the surface coat considerably changes the performance of SPIONs as MRI contrast agents [10, 11]. The nano-scale size of SPIONs (<100 nm) would allow the conjugation with many molecular markers, which interact at cellular and molecular levels. As a result, an ever increasing trend of disease targets is offered for molecular imaging [9]. Recently, due to the great potential applications in biomedical area, extensive works have been focused on the preparation of Fe_3O_4NPs and modification of their surface with preferred properties. Surface coating of magnetite NPs should provide stability, biocompatibility and non-toxicity in biological media [12-15]. Hence, the surface coats should be biocompatible, biodegradable, and water-dispersible materials. Polysaccharides are one of the most common surface coatings which are used for the modification of magnetic NPs, and include agarose, dextran, chitosan, alginate, heparin, carrageenan, pullulan, hyaluronic acid and starch [16, 17]. Dextran is a branched polymer of glucose molecules in which the units of α-linked *D*-glucopyranosyl are repeated to form the linear backbone. This type of polymer can be toughly physisorb on the surface of Fe_3O_4NPs in the alkaline solutions to produce enmeshed NP cores *via* non-covalent interactions of the abundant hydroxyl groups. Then, the hydroxyl groups of dextran can be easily cross-linked and functionalized using primary amines to attach to a wide range of target compounds such as ligands, peptides, or probes [18-27].

Recently, many efforts have been carried out in the development of different wet chemical processes for the synthesis of superparamagnetic NPs, which include such as sol-gel [26], solvothermal [27], hydrothermal [28], precipitation [29-32], solid state reactions [33] and thermal decomposition [34,35]. Although these synthetic methods have been improved during a few past decades, however, control of the particle size of SPIONs and their distribution are still problematic issues that should be solved. For example, it is difficult and vitally important to control the formation process of products in chemical precipitation which affords NPs with a broad size distribution, irregular morphology, mixed phase (i.e. Fe_3O_4 with γ-,α-Fe_2O_3) and aggregated form. Moreover, decomposition process as a chemical synthetic method requires higher temperature (100-300 °C), toxic and expensive precursors, and exhibits limited controllability of the particle size and morphology. These are the main reasons that some alternative methods such as the electrochemical procedure should be developed. One of the most promising alternative techniques for the preparation of NPs is the electrodeposition method. In this method, the composition, crystallinity, purity, particle size and deposit properties can be effectively controlled by manipulating or adjusting the applied direct current and/or the potential into the system [36-44]. Until now, both anodic and cathodic deposition techniques have been used for the preparation of SPIONs [45-53]. Many works have been performed on the anodic deposition of SPIONs [44-50]. The results of these works have shown that the anodic deposition has two critical requirements, which are: (i) applying the high voltage (40-62 V) [47, 48] and (ii)appropriate distance (<5 cm) between the anodic and cathodic electrodes [46-48]. In addition, this method usually needs supporting electrolyte and/or surfactant [44, 45], and in some cases, products are mixed iron oxide phases [44, 47, 48]. In contrast, the cathodic deposition has not any practical crises and also no need to surfactant or supporting electrolyte. It seems that CED method could solve suffers related to the anodic deposition disadvantages. However, there are only a few reports in literature about the CED preparation of Fe_3O_4NPs*via* a base electrogeneration process [50-53].Verelst *et al.*[52], for the first time, conducted the basic research about the CED process of Fe_3O_4 NPs in the ethanol solution. They found out that the CED method provides mono-dispersed SPIONs with controlled size without using any stabilizing agent or micelles for preventing agglomeration of NPs [52, 53]. As a result, the preparation of SPIONs *via* CED route can be considered as an alternative route to overcome to the mentioned problems.

Recently, we applied CED method for the preparation of iron oxide NPs and reported that naked and polymer coated SPIONs can be efficiently prepared through this route [53-58]. In this work, we report the one step CED synthesis of dextran coated Fe_3O_4 NPs in aqueous media. The

obtained results showed that dextran coated Fe_3O_4 NPs with suitable size have appropriate magnetic properties. To the best of our knowledge, the one-step CED process for the preparation of dextran coated SPIONs has not been reported until now.

MATERIAL AND METHODS

Materials

Ferrous chloride tetrahydrate ($FeCl_2{\cdot}4H_2O$, 99%), ferric nitrate nonahydrate ($Fe(NO_3)_3{\cdot}9H_2O$, 99.9%), and dextran (M_w~70000) were purchased from the Sigma Aldrich Company. All materials were used as received.

Preparation of naked Fe_3O_4NPs

Magnetite (Fe_3O_4) NPs were synthesized *via* a facile cathodic electrodeposition method. In this procedure, a two-electrode electrochemical cell was used in all the electrodeposition experiments. The stainless-steel sheet (316 L, 5 cm×5 cm×0.5 mm) was applied as the cathode and graphite plate was used as the anode. Prior to each deposition, the cathode sheets were polished in the two-electrode system, including lead (Pb) sheets and steel sheet is at the working electrode. The composition of electropolishing bath was phosphoric acid and sulfuric acid with the ratio of 50:25 v/v and the balanced deionized water, and the temperature was adjusted at 70°C [59]. The electropolishing process of steel sheets was performed at the direct current with the density of 0.5 A cm^{-2} for 10 min. Then, the steel sheets were washed for several times with the deionized water and used as the cathode in the CED synthesis of the Fe_3O_4NPs. The electrodeposition of NPs was conducted on an electrochemical workstation system (Potentiostat/Galvanostat, Model: NCF-PGS 2012, Iran). The aqueous solution of $FeCl_2$:$Fe(NO_3)_3$ (0.01 M) with molar ratio of 1:2 was used as the electrodeposition bath. Naked Fe_3O_4 NPs were synthesized by galvanostatic electrodeposition using the direct current density of 10 mA cm^{-2}. The bath's temperature and deposition time were 25°C and 30 min, respectively. After electrodeposition process and washing the steel cathode several times with distilled water, the deposited black film was scraped from the cathode surface and then was dried at 70°C in vacuum oven for 5h. Finally, the dried black powder was obtained and evaluated by different characterization analyses.

Preparation of dextran coated NPs

In situ one-step surface coating was applied for the preparation of dextran coated of Fe_3O_4 NPs. In fact, a dextran layer was coated on the surface of Fe_3O_4 NPs during their CED preparation procedure. To aim this purpose, the same electrochemical conditions, which were applied for the preparation of naked NPs, were used here. Only 1 g L^{-1} dextran as coating agent was added to the electrolyte bath, and the CED process was followed. After this step, the steel electrode was rinsed for several times with distilled water and dried at 70°C for 5 h. Also, the deposits were scraped from the substrates and centrifuged at 6000 rpm for 20 min in order to removal of weekly bounded dextran attached to the NPs' surface.

Characterization of NPs

Crystal phase, structure and morphometric analyses

A field emission scanning electron microscopy (FE-SEM, Mira 3-XMU) was used to observe the size and morphology of the prepared NPs. Transmission electron microscopy (TEM, Phillips EM 208 with an accelerating voltage of 100 kV) was also used towards the better determination of NPs' size. The XRD patterns of the prepared NPs were obtained by X-ray diffraction of powder (XRD, Phillips Model X'PERT MPD with Co Kα radiation (λ=1.789 Å)). The crystallite size was also calculated using Scherrer equation and diffraction patterns of XRD analysis. Also, hydrodynamic diameter and zeta potential of the prepared naked and dextran coated NPs were determined by dynamic light scattering (DLS, 4700 Malvern Instruments, UK). These measurements were conducted on the as-prepared dispersions of the naked and the coated NPs (with the concentration of 0.1 mg/L of Fe cations) without any filtration or centrifugation.

Surface characterization

FT-IR, thermogravimetric, dynamic light scattering (DLS) and zeta-potential analyses were used to identify the dextran coating on the surface of the electrodeposited NPs. FT-IR spectra were obtained using a Bruker Vector 22 Fourier transformed infrared spectroscope. Each FTIR spectrum was collected after 20 scans at a resolution of 4 cm^{-1} from 400 to 4000 cm^{-1}. Thermal behavior (DCS-TG) analysis was carried out in N_2 atmosphere between room temperature and 600°C at a heating rate of 5°C min^{-1} using a thermoanalyzer (STA-1500).

Hydrodynamic diameter and zeta potential of the prepared NPs were determined by dynamic light scattering (DLS, 4700 Malvern Instruments, UK) at 632 nm of wavelength laser in the aqueous electrolyte. The results were obtained with a theoretical refractive index of magnetite 2.42, and analyzed by the cumulant method as intensity distribution diagrams.

Characterization of magnetic properties

The magnetic properties of the prepared naked and dextran coated NPs were determined using vibrating sample magnetometer (VSM, Meghnatis Daghigh Kavir Co., Iran). Also, the magnetic hysteresis and saturation magnetization of both the naked and dextran coated NPs were evaluated and compared with each other.

RESULT AND DISCUSSION

XRD analysis

The representative XRD patterns of the naked Fe_3O_4 and dextran coated Fe_3O_4 *via* CED process are shown in Fig. 1. Both diffraction peaks corresponding to Fe_3O_4 have been observed, indexed to (111), (220), (311), (400), (442), (511) and (440) planes of a cubic unit cell (JCPDS 01-088-0315, a=0.83980 nm). It was confirmed that under the applied electrochemical conditions magnetite particles with a single phase are electrodeposited. Also, it should be noted that we previously found that the pure magnetite NPs with size of ~10 nm can be synthesized *via* galvanostatic deposition in ethanol [56] and aqueous media [57]. From XRD pattern, it is seen that the intensity of the crystallization peak of Fe_3O_4 coated with dextran, was lower in comparison with the uncoated Fe_3O_4 NPs due to the existence of dextran on the surface of Fe_3O_4NPs. Notably, a little difference is observed in the main diffraction peaks of both prepared samples. The difference between XRD diffraction peaks can be attributed to the smaller crystallite size of prepared NPs. The average crystallite size (D) of both prepared NPs was calculated using the diffraction line-width of XRD patterns, based on Scherrer's equation ($D=0.9\lambda/\beta \cos(\theta)$), where, β is the full width at half maximum (FWHM) of the (311) peak. The calculations revealed that the naked and dextran coated NPs have sizes of 7.2 and 8.4 nm, respectively. It is worthwhile noting that electrochemical preparation of dextran coated magnetite in aqueous solution *via* base electrogeneration has not been reported until now.

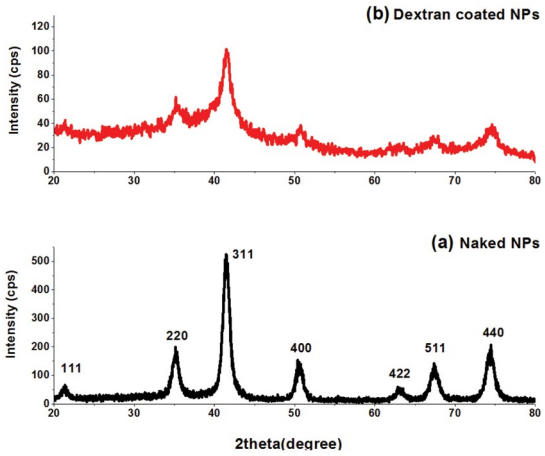

Fig. 1. XRD patterns of the electrodeposited samples.

Morphological evaluation

Morphological characteristics of the prepared NPs were specified by FE-SEM and TEM observations. The FE-SEM images of the naked and dextran coated NPs are illustrated in Fig. 2. It is clearly seen that both samples have granular morphology and no serious aggregation is observed. Comparing the FE-SEM images showed that the dextran coated Fe_3O_4 NPs sample has better particle's shape and well-dispersed texture than the naked Fe_3O_4 sample. In fact, the naked Fe_3O_4 exhibits more agglomerated particles which are stuck together. In contrast, dextran coated Fe_3O_4 has more uniform particles and exhibits no obvious agglomerated morphology. As depicted in FE-SEM images, the average diameter of both samples is estimated to be 10 nm. For better determination of size and morphology of particles, high magnification TEM images were performed for the prepared NPs. TEM images disclosed that both samples have a fine particle morphology at nano scale. As completely obvious in the TEM images (Fig. 3), the dextran coated NPs have proper dispersion in comparison with the naked ones. This observation indicated that the *in situ* dextran coating Fe_3O_4 during electrosynthesis process prevents them to stick with each other. Significantly, the aggregated form of SPIONs prevents them to exhibit the behavior of single particles and the advantages of the nanometer size. As it can be seen that from TEM images, the size of naked and dextran coated Fe_3O_4 NPs were ~8 nm and ~12 nm, respectively.

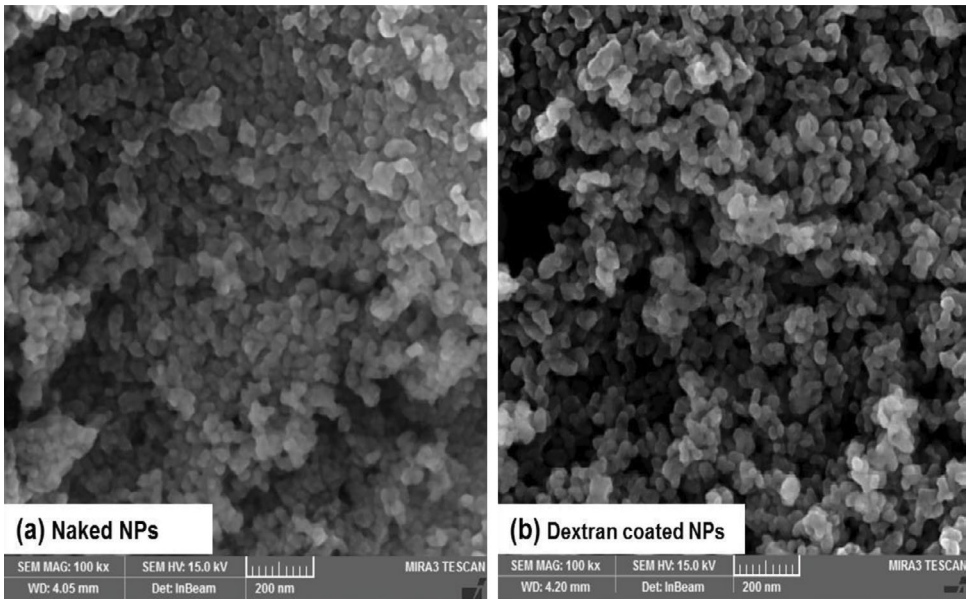

Fig. 2. FE-SEM images of the electrodeposited samples.

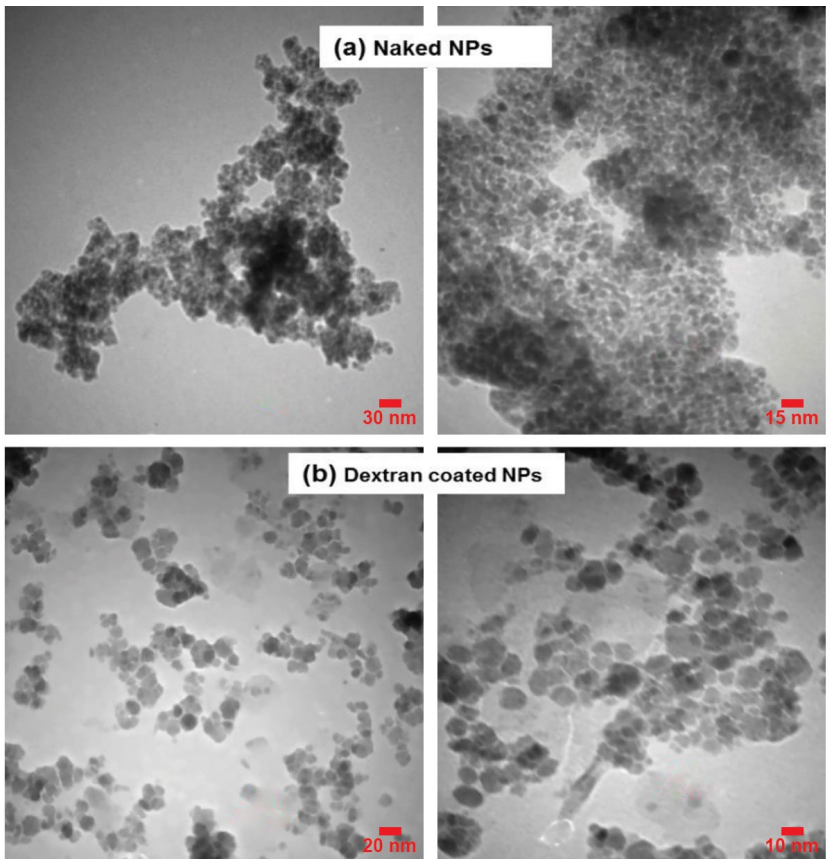

Fig. 3.TEM images of the electrodeposited samples.

FT-IR analysis

FT-IR is an appropriate technique for the investigation of the chemical adsorption or chemical interaction. In this research, FT-IR studies of the prepared Fe_3O_4NPs were carried out to analyze the surface's properties of the Fe_3O_4NPs. The FT-IR spectra of the naked and the dextran coated Fe_3O_4 NPs are presented in Fig. 4. The characteristic peaks of magnetite are observed at 421 cm^{-1} (due to the ν_1 stretching vibration of Fe-O bond [55]) and 556 and 615 cm^{-1} (due to the ν_2 stretching vibrations of Fe-O bond [15,55]) for the naked NPs, respectively, which confirmed magnetite phase of electrodeposited samples. For the coated sample, the main vibration of Fe-O bond is seen at about 578 cm^{-1}, which shows a blue shift as compared with Fe-O vibrations in naked NPs. This shift implicates the change in the environment of the NPs after coating, where the new band between Fe_3O_4 NPs surface and dextran coat is formed. For the naked NPs, the peaks, observed at 3427 cm^{-1} and 1639 cm^{-1}, related to the vibration mode of hydroxyl groups on the surface of NPs [20-25]. The comparison of the naked and dextran coated NPs' spectra showed some new absorption bands. For instance, (i) a wide peak between 3700 and 3200 cm^{-1} indicates the structural OH in the dextran chains [24,26], (ii) the bands at 2931 and 2894 cm^{-1} are related to asymmetrical and symmetrical stretching vibration of C-H in CH_2 group, respectively, (iii) the bands at about 1460, 1356 and 1262 cm^{-1} are due to the deformation vibrations of H-C-OH in the dextran chains, (iv) the band of O-H vibration modes are placed at 864 and 1016 cm^{-1}, (v) the band at 1637 cm^{-1} is attributed to the bending vibration of C–H bond in CH_3 group, and (vi) the asymmetrical and symmetrical vibrations of C-O-C can be found at 1152 and 846 cm^{-1}, respectively [24,25]. These peaks are the main absorption bands regarding to dextran, and completely proved that the surface of NPs has been covered with the dextran [25,26]. It is believed that different interactions keep dextran on the surface of Fe_3O_4 NPs such as van der Waals force, hydrogen bond, and electrostatic interactions [25-27].

Dynamic light scattering (DLS)

The hydrodynamic diameter of the prepared NPs (i.e. both naked and dextran coated) were measured by using the DLS analyzer. Fig. 5 illustrates the distributions of particle size in the naked and dextran coated NPs. For naked NPs, the average hydrodynamic diameter was ~17 nm, while this diameter was 54 nm for the dextran coated NPs. This increase of size completely implicates the presence of polymer coat on the surface of iron oxide NPs. Zeta-potential measurement was also applied to determine the surface charge of electrodeposited NPs. The measurements showed that naked NPs have a negative zeta-potential of -26.7 mV, where the dextran coated NPs have the zeta potential of -2.1 mV. The change in surface charge of NPs clearly implicated the surface coating of NPs with dextran during their electrodeposition process. Also, surface coating of NPs with dextran caused a significant decrease in the amount of zeta-potential. It is believed that the negative value of zeta-potential for Fe_3O_4 NPs rises from the existence of OH^- groups on the surface of NPs [25-27]. Thus, reduction of surface charge after coating the Fe_3O_4 NPs with dextran can be an evidence of hydrogen bonding between the oxygen of dextran and the hydroxyl group of NPs.

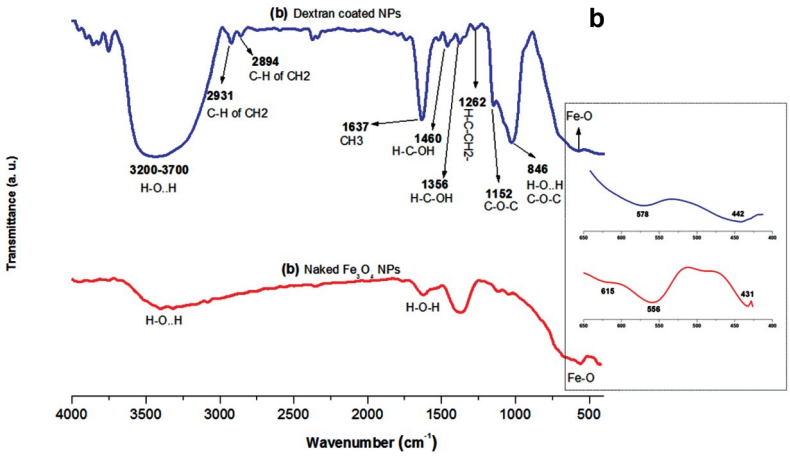

Fig. 4. IR spectra of (a) the naked and (b) the dextran coated Fe_3O_4 NPs.

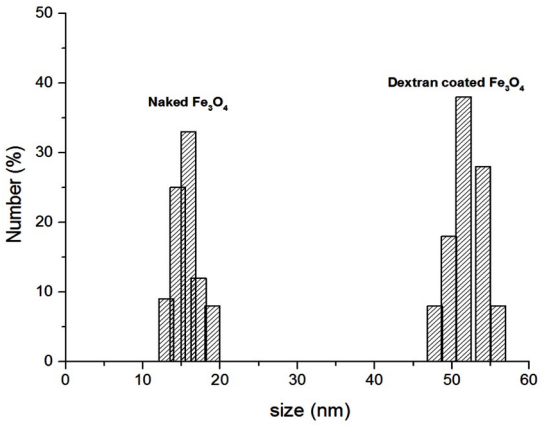

Fig. 5. Hydrodynamic diameter distribution for naked and dextran coated Fe_3O_4 NPs.

Thermogravimetric analysis

Thermogravimetric behavior of the naked and dextran-coated NPs was studied in the temperature range of 25-600°C, and the both corresponding DSC and TGA diagrams are shown in Fig. 6. The naked Fe_3O_4 NPs are thermally stable and no special endo and/or exothermic peaks are observed in the DSC diagram (Fig.6a), and correspondingly there is no significant weight loss in TGA diagram (Fig. 6b). TGA diagram exhibits only 1.5% weight loss for uncoated NPs, where the most portion of this weight loss occurs in the temperature range of 25 to 200°C. So, this weight loss is related to the removal of the hydroxyl groups attached on the surface of Fe_3O_4NPs [22-24,57]. It was clear from the diagrams that the surface of Fe_3O_4NPs was effectively covered with hydroxyl groups during their synthesis in the aqueous solution [24,60]. Moreover, the IR analysis (in Fig. 4b) clearly proved the presence of hydroxyl groups on the surface of naked NPs. For dextran coated NPs, DSC diagram has a multistep exothermic peak in the temperature range of 200 to 350°C (Fig. 6a), which is completely in agreement with the ones reported in literature [24-27,61-64]. Respectively, TGA diagram shows a major weight loss in this temperature range. It was reported that free dextran exhibits three distinct degradation stages [63,64]; (i) elimination of the adsorbed water at 80-90°C results in the weight loss of ~10%, (ii) the breakdown of organic skeleton at 245-250°C with the total weight loss of 70%, and (iii) complex degradation process in the temperature range of 330 to 495°C with the total weight loss of 100% [61-64]. It was also reported that the degradation stages of dextran coated NPs are occurred at 70-80°C and 280-290°C with the weight loss of ~4% and ~20%, respectively. At around 490°C, a total weight loss is observed which indicates the complete dissociation of dextran from the NPs' surface [25,61,62]. For prepared dextran coated NPs, the first degradation stage is observed at the range of 50-120°C with the weight loss of 11.7%, and the second stage is seen at higher temperature (i.e. 150-250°C) with a strong exothermic peak at 230°C. TGA diagram indicates the weight loss of 19.3% for this stage. Notably, this sharp endothermic peak shows some shift in comparison with those of free dextran [25,27], which is related to the catalytic effect of iron. The third stage is occurred in the temperature range of 250-500°C with a weight loss of 7.3%. The total percentage of dextran coated on the surface of NPs is estimated to be 38.3%.

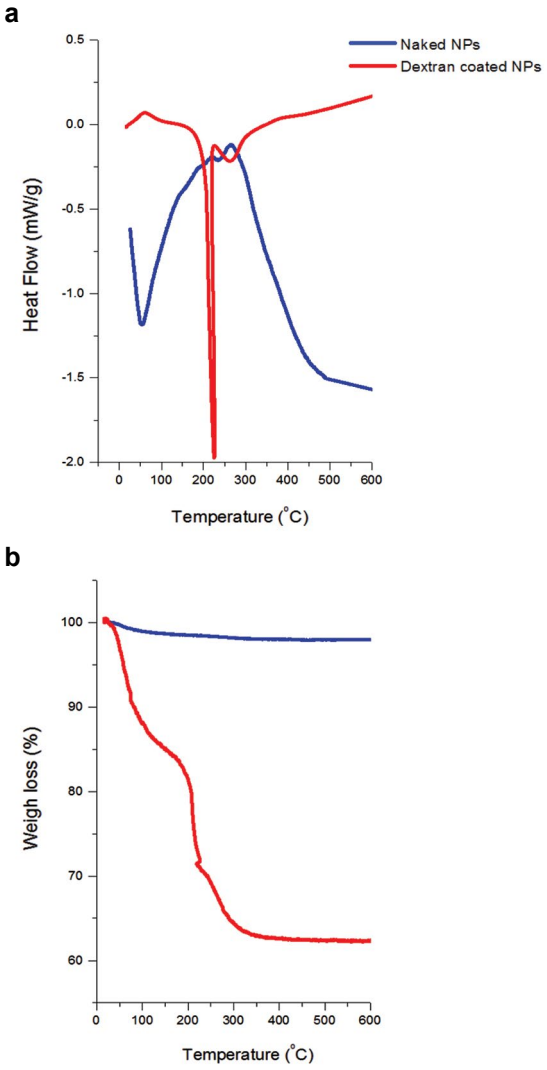

Fig. 6.Thermogravimetric behavior of the prepared NPs between temperature of 25 and 600°C; (a) DSC and (b) the related TG curves.

Magnetic evaluation

For separation and hyperthermia applications, it is important that magnetic NP retain their favorable magnetic properties after modification with non-magnetic polymer. The diagram of magnetic behavior, i.e. magnetizations (M) versus applied magnetic field (H) of both naked and dextran coated iron oxide NPs was investigated by VSM as shown in Fig. 7. As evident from the both diagrams, prepared NPs exhibit superparamagnetic properties at room temperature (Fig. 7). The naked Fe_3O_4 NPs have saturation magnetization (M_s) value of M_s=82.3 emu g^{-1} with remnant magnetization (M_r) of 0.71 emu g^{-1} and coercivity (*Ce*) of 2.3 *Oe*. These data indicated the suitable magnetic behavior of the electrodeposited magnetite NPs. However, the dextran coated NPs shows the M_s value of 43.1 $emug^{-1}$ with M_r=0.47 $emug^{-1}$ and *Ce*=0.81*Oe*. These magnetic data are comparable with those reported for dextran coated NPs prepared through other methods. For example,M_s=12.1 emu g^{-1}, M_r=0.01 emu g^{-1} and *Ce*=0.83*Oe*forNPs prepared by co-precipitation method [18], M_s=12.1 emu g^{-1}fordextran coated SPIONs prepared by co-hydrothermal method [20], M_s=38.7 emu g^{-1}fordextran coated NPs fabricated by co-precipitation method [30] and M_s=70.2 emu g^{-1}fordextran coated NPs synthesized by co-precipitation method [31]. Furthermore, it was seen that the magnetization of iron oxide NPs decreases by coating with dextran. This decrease in the saturated magnetization could be ascribed to the reduction of magnetite fraction by 30%wt. in the dextran coated NPs, as confirmed by DSC-TG analysis (Fig. 6). In comparison with the naked NPs, the coated ones displayed negligible *Mr* and *Ce* values which reveal their better superparamagnetic nature. These results may originate from their better dispersibility and not agglomerated form (as depicted in TEM images in Fig. 3). As reported in the literature [34-39], the prepared NPs can act as the single magnetic domains and soft magnetic materials in the presence of magnetic field. As a result, these dextran-coated NPs can be suitable for biomedical applications such as hyperthermia.

CED mechanism and in situ surface coating

The schematics of deposition of Fe_3O_4NPsthrough CED and their surface coating are shown in Fig. 8. Formation and deposition of the magnetite on the cathode surface, from the Fe chloride/nitrate bath can be described on the base of a two-step procedure as schematically shown in Fig. 8a [35, 44, 56]:

- OH^- electrogeneration step:

$$NO_3^- + 2H_2O + 2e^- \rightarrow NO_2^- + 2OH^- \quad (1)$$

E^o = -0.32 V vs. Ag/AgCl

$$2H_2O + 2e^- \rightarrow H_2 + 2OH^- \quad (2)$$

E^o = −1.08 V vs. Ag/AgCl

where the pH of the solution increases near the surface of the steel electrode resulting the deposition of the oxide NPs as the OH^- concentration increased.

- Deposit formation step:

$$Fe^{3+}(aq) + Fe^{2+}(aq) + 6OH^-(aq) \rightarrow Fe_3O_4 + 3H_2O \quad (3)$$

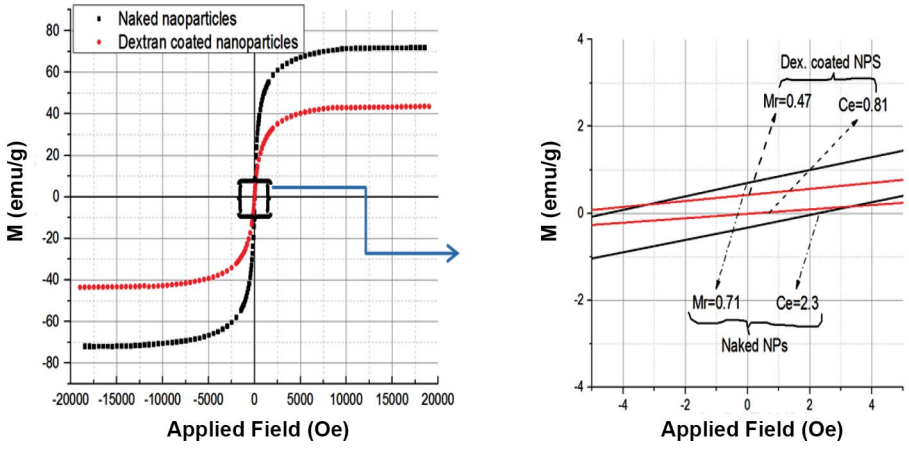

Fig. 7. Hysteresis curves of the naked and dextran coated iron oxide NPs.

Considering the value of the observed potential (-1.05 V *vs.* Ag/AgCl at the applied current density of 10 mA cm^{-2})) during the CED process, it is accepted that the reduction of water (Eq. (2)) has a major role in the base electrogeneration step. In fact, the electrochemical step proceeds through reactions of (1) and (2) during the deposition process, as shown schematically in the inset of Fig. 8a. Furthermore, the flow of gas bubbles was observed on the surface of cathode throughout the deposition step, which further confirmed the electrogeneration of OH^- ions via H_2O molecules reduction. In the chemical step, Fe^{3+} and Fe^{2+} cations are reacted with the OH^- ions to produce Fe_3O_4 deposit, as schematically shown in the inset of Fig. 8a. When the dextran polymer is added into the deposition bath, the cathodic electrodeposition of Fe_3O_4 is also preceded via the above mentioned mechanism, and the pure phase of magnetite NPs with the polymer layer on their surfaces is obtained as confirmed by XRD, IR, TEM and DSC-TGA analyses. In fact, the structural and morphological analyses of the deposited prepared in the presence of dextran revealed that the CED mechanism and products were not affected by the addition of the dextran to the bath. Fig. 8b shows a schematic of the Fe_3O_4deposition in the presence of dextran. In the electrodeposition presence, it is anticipated that dextran molecules would move electrophoretically towards the cathode electrode when the electrosynthesis is started. However, the Fe_3O_4 NPs formed on the surface of cathode have hydroxyl groups on their surfaces (as confirmed by zeta potential measurements and IR analysis) and dextran molecules could bounded into the Fe_3O_4 cores through hydrogen bonding. Hence, the obtained deposit i.e. Fe_3O_4 NPs are surface coated with dextran during their deposition as confirmed by IR, DLS and TG analyses.

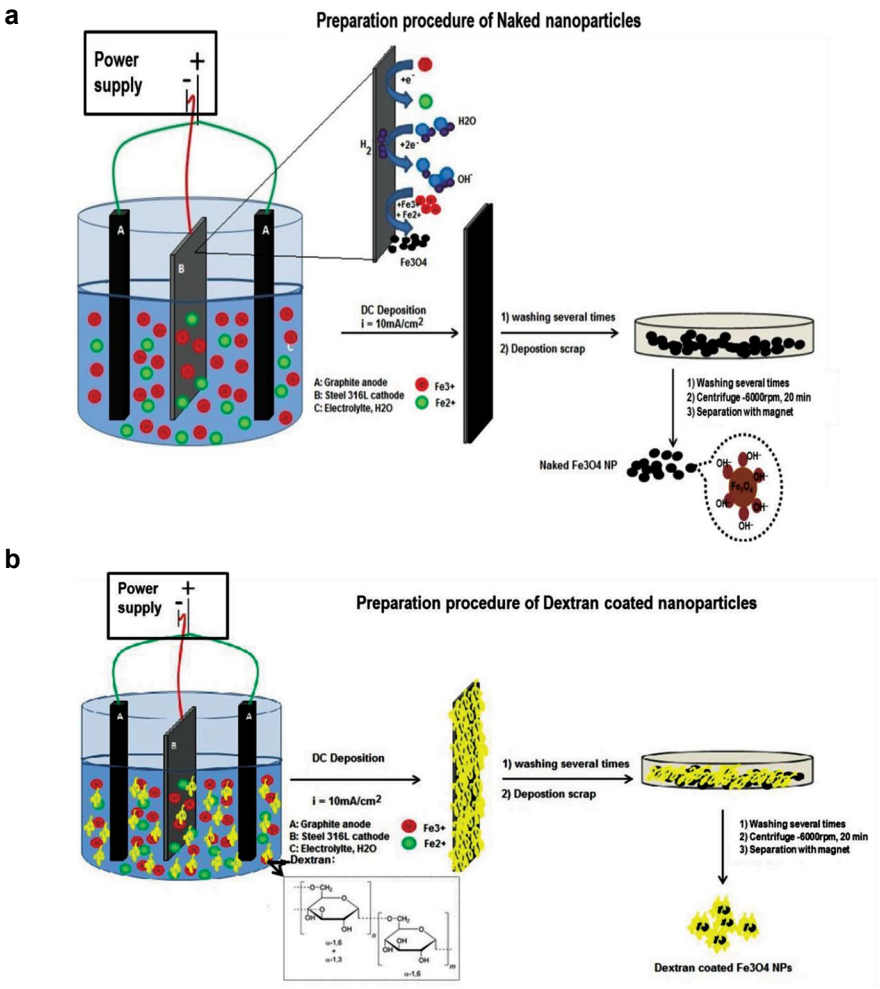

Fig. 8.Schematic view of CED procedure for preparation of (a) naked and (b) dextran coated Fe_3O_4NPs.

CONCLUSION

Naked and dextran-coated NPs of iron oxide with magnetite phase were prepared in aqueous electrolyte solution *via* a one-step cathodic electrochemical deposition (CED) route without using any surfactant or supporting electrolytes. Morphological observations through FE-SEM and TEM displayed that the prepared Fe_3O_4 and dextran-coated Fe_3O_4 samples have well-dispersed NPs with the size of 10 nm. TG, DLS and FT-IR analyses were used to confirm the presence of dextran on the surface of NPs. The prepared NPs have appropriate size and magnetic properties which are suitable for biomedical applications. Finally, it was found that cathodic electrochemical deposition can be regarded as a new platform for the effective preparation of dextran coated Fe_3O_4 NPs.

CONFLICT OF INTEREST

The authors declare that there is no conflict of interest regarding the publication of this paper.

REFERENCES

1. E. Tombacz, R. Turcu, V. Socoliuc, L. Vekas, Biochem. Biophys. Res. Commun. 468, 442–453 (2015).
2. C. Scialabba, R. Puleio, D. Peddis, G. Varvaro, P. Calandra, G. Cassata, L. Cicero, M. Licciardi, G. Giammona, Nano Res. 10, 3212–3227 (2017).
3. E. C. Abenojar, S. Wickramasinghe, J. Bas-Concepcion, A. C. S. Samia, Prog. Nat. Sci. 26, 440–448 (2016).
4. R. A. Revia, M. Zhang, Mater. Today 19, 157-168 (2016).
5. Y. Huang, K. Mao, B. Zhang, Y. Zhao, Mater. Sci. Eng. C 70, 763–771 (2017).
6. M. Aghazadeh, I. Karimzadeh, Curr. Nanosci. doi:10.2174/1573413713666170825113906, (2017).
7. J. M. Poller, J. Zaloga, E. Schreiber, H. Unterweger, C. Janko, P. Radon, D. Eberbeck, L. Trahms, C. Alexiou, R. P. Friedrich, Int. J. Nanomedicine 12, 3207–3220 (2017).
8. F. M. Kievit, M. Zhang, Acc. Chem. Res. 44, 853–862 (2011).
9. E. Blanco, H. Shen, M. Ferrari, Nat. Biotechnol. 33, 941–951 (2015).
10. M.H. Hsiao, Q. Mu, Z. R. Stephen, C. Fang, M. Zhang, ACS Macro Lett. 4, 403-407 (2015).
11. S. Tambalo, L. Peruzzotti-Jametti, R. Rigolio, J. Neurosci. 35, 10088–10100 (2015).
12. K. Hola, Z. Markova, G. Zoppellaro, J. Tucek, R. Zboril, Biotechnology Adv. 33, 1162–1176 (2015).
13. Z. Zhou, C. Wu, H. Liu, X. Zhu, Z. Zhao, L. Wang, Y. Xu, H. Ai, J. Gao, ACS Nano 9, 3012–3022 (2015).
14. I. Karimzadeh, M. Aghazadeh, T. Doroudi, M. R. Ganjali, P. H. Kolivand, and D. Gharailou, Curr. Nanosci. 3, 274-280 (2017).
15. M. Peng, H. Li, Z. Luo, J. Kong, Y. Wan, L. Zheng, Q. Zhang, H. Niu, A. Vermorken, W.van de Ven, Nanoscale 7, 11155–11162 (2015).
16. A. Sabareeswaran, E. Beeran Ansar, P. R. V. Harikrishna Varma, P. Vilappil Mohanan, T. Variathu Kumary, Nanomedicine 12, 1523-1533 (2016).
17. A. Basu, K. R. Kunduru, E. Abtew, A.J. Domb, Bioconjugate Chem. 26, 1396–1412 (2015).
18. Z. Shaterabadi, G. Nabiyouni, M. Soleymani, Mater. Sci. Engin. C 75, 947-956 (2017).
19. A. K. Hauser, R. Mathias, K. W. Anderson, J. Zach Hilt, Mater. Chem. Phys. 160, 177-186 (2015).
20. G. B. da Silva, M. Marciello, M. del Puerto Morales, C.J. Serna, M.D. Vargas,C. M. Ronconi, J. Braz. Chem. Soc. 28, 731-739 (2017).
21. N.S. Remya, S. Syama, A. Sabareeswaran, P.V. Mohanan, Int. J. Pharmaceut. 511, 586-598 (2016).
22. D. G. You, G. Saravanakumar, S. Son, H. S. Han, R. Heo, K. Kim, I. C. Kwon, J. Y. Lee, J. H. Park, Carbohydrate Polym. 101, 1225–1233 (2014).
23. R. Y. Hong, J. H. Li, J. M. Qu, L. L. Chen, H. Z. Li, Chem. Engin. J. 150, 572–580 (2009).
24. M. Khalkhali, S. Sadighian, K. Rostamizadeh, F. Khoeini, M. Naghibi, N. Bayat, M. Habibizadeh, M. Hamidi, Bioimpacts 5, 141–150 (2015).
25. M. Peng, H. Li, Z. Luo, J. Kong, Y. Wan, L. Zheng, Q. Zhang, H. Niu, A. Vermorken, W. Van de Ven, C. Chen, X. Zhang, F. Li, L. Guo, Y. Cui, Nanoscale 7, 11155-11162 (2015).
26. D. Jinmori, Y. Masubuchi, S. Kikkawa, Mater. Res. Bulletin 88, 214-217 (2017).
27. B. Yang, X. Yang, X. Li, Y. Cao, R. Yu, J. Magn. Magn. Mater. 405, 22-27 (2016).
28. S. Gyergyek, D. Makovec, M. Jagodič, M. Drofenik, H. Hofmann, J. Alloys Compd. 694, 261-271 (2017).
29. L. Shen, Y. Qiao, Y.Guo, S. Meng, G. Yang, M. Wu, J. Zhao, Ceram. Int. 40, 1519-1524 (2014).
30. R.Y. Hong, B. Feng, L.L. Chen, G.H. Liu, H.Z. Li, Y. Zheng, D.G. Wei, Biochem. Engin. J. 42, 290–300 (2008).
31. M. Khalkhali, K. Rostamizadeh, S. Sadighian, F. Khoeini, M. Naghibi, M. Hamidi, Daru J. Pharmaceut. Sci. 23, 45-51 (2015).
32. S. Lin, K. Lin, D. Lu, Z. Liu, J. Environmental Chem. Engin. 5, 303-309 (2017).
33. R. Hufschmid, H. Arami, R. M. Ferguson, M. Gonzales, E. Teeman, L. N. Brush, N. D. Browning, K. M. Krishnan, Nanoscale 7, 11142-11154 (2015).
34. D. Stanicki, L. Vander Elst, R. N. Muller, S. Laurent, Curr. Opinion Chem. Engin. 8, 7–14 (2015).
35. W. Glasgow, B. Fellows, B. Qi, T. Darroudi, C. Kitchens, L. Ye, T. M. Crawford, O. T. Mefford, Particuology 26, 47-53 (2016).
36. M. Aghazadeh, M.R. Ganjali, P. Noruzi, Thin Solid Films 634, 24-32 (2017).
37. M. Aghazadeh, M.R. Ganjali, J. Mater. Sci.: Mater. Electron. 28, 8144–8154 (2017).
38. A. Barani, M. Aghazadeh, M. R. Ganjali, B. Sabour, A. A. M. Barmi, S. Dalvand, Mater. Sci. Semicond. Proc. 23, 85-92 (2014).
39. M. Aghazadeh, S. Dalvand, M. Hosseinifard, Ceram. Int. 40, 3485-3493 (2014).
40. M. Aghazadeh, M. Asadi, M.G. Maragheh, M.R. Ganjali, P.

Norouzi, F. Faridbod, Appl. Surf. Sci. 364, 726-731 (2016).

41. M. Aghazadeh, M.R. Ganjali, P. Norouzi, J. Mater. Sci.: Mater. Electron. 27, 7707–7714 (2016).
42. M. Aghazadeh, B. Sabour, M. R. Ganjali, S. Dalvand, Appl. Surf. Sci. 313, 581-584 (2014).
43. M. Aghazadeh, M.G. Maragheh, M.R. Ganjali, P. Norouzi, F. Faridbod, Appl. Surf. Sci. 364, 141-147 (2016).
44. J. Tizfahm, M. Aghazadeh, M. Ghannadi Maragheh, M. R. Ganjali, P. Norouzi, F. Faridbod, Mater. Lett. 167, 153-156 (2016).
45. A. Rodrıguez-Lopez, A. Paredes-Arroyo, J. Mojica-Gomez, C. Estrada-Arteaga, J. J. Cruz-Rivera, C. G. Elıas Alfaro, R. Antano-Lopez, J. Nanopart. Res. 14, 993-1001 (2012).
46. F. Fajaroh, H. Setyawan, W. Widiyastuti, S. Winardi, Adv. Powder. Technol. 23, 328–333 (2012).
47. M. Starowicz, P. Starowicz, J. Zukrowski, J. Przewoznik, A. Lemanski, C. Kapusta, J. Banas, J. Nanopart Res. 13, 7167-7176 (2011).
48. N. Salamun, H. X. Ni, S. Triwahyono, A. Abdul Jalil, A. Hakimah Karim, J. Fundamental Sci. 7, 89-92 (2011).
49. M. Aghazadeh, I. Karimzadeh, M.R. Ganjali, M. MohebiMorad, Mater. Lett. 196, 392-395 (2017).
50. D. Carlier, C. Terrier, C. Arm, J. P. Ansermen, Electrochem. Solid-State Lett. 8, 43–46 (2005).
51. H. M. Kothari, E. A. Kulp, S. J. Limmer, P. Poizot, E. W. Bohannan, J. A. Switzer, J. Mater. Res. 21, 293-301 (2006).
52. R. F. C. Marques, C. Garcia, P. Lecante, S. J. L. Ribeiro, L. Noe, N. J. O. Silva, V. S. Amaral, A. Millan, M. Verelst, J. Magn. Magn.Mater. 320, 2311–2315 (2008).
53. M. Ibrahim, K.G. Serrano, L. Noea, C. Garcia, M. Verelst, Electrochim. Acta 55, 155-158 (2009).
54. I. Karimzadeh, M. Aghazadeh, M. R. Ganjali, P. Norouzi, S. Shirvani-Arani, T. Doroudi, P. H. kolivand, S. A. Marashi, D. Gharailou, Mater. Lett. 179, 5-8 (2016).
55. I. Karimzadeh, M. Aghazadeh, T.Dourudi, M.R. Ganjali, P.H. Kolivand, Curr.Nanosci.13, 167-174 (2017).
56. M. Aghazadeh, Mater. Lett. 211, 225-229 (2018).
57. I. Karimzadeh, M. Aghazadeh, M.R. Ganjali, P. Norouzi, T. Doroudi, P.H. Kolivand, Mater. Lett. 189, 290-294 (2016).
58. I. Karimzadeh, H. Rezagholipour Dizaji, M. Aghazadeh, Mater. Res. Express 3, 095022 (2016).
59. F. Khosrow-pour, M. Aghazadeh, B. Sabour, S. Dalvand, Ceram. Int. 39, 9491-9498 (2013).
60. J.TalatMehrabad, M. Aghazadeh, M. Ghannadi Maragheh, M. R. Ganjali, P. Norouzi, Mater. Lett. 184, 223-226 (2016).
61. O. Carp, L. Patron, D. C. Culita, P. Budrugeac, M. Feder, L. Diamandescu, J. Thermal Anal. Calorimetry 101, 181-187 (2010).
62. A. K. Hauser, R. Mathias, K. W. Anderson, J. Zach Hilt, Mater. Chem. Phys. 160, 177-186 (2015).
63. A. Saraswathy, S. S. Nazeer, N. Nimi, S. Arumugam, S. J. Shenoy, R. S. Jayasree, Carbohydrate Polym. 101, 760-768 (2014).
64. A. Jurikova, K. Csach, J. Miskuf, M. Koneracka, V. Zavisova, M. Kubovcikova, P. Kopcansky, Acta Phys. Polonica A 121, 1296-1298 (2012).